ISBN: 978-3-95450-231-8 ISSN: 2673-5490 doi: 10.18429/JACoW-IPAC2023-TUPL025

SLICE ENERGY SPREAD MEASUREMENTS IN THE EUROPEAN XFEL INJECTOR

S. D. Walker*, S. Tomin, I. Zagorodnov
Deutsches Elektronen-Synchrotron DESY, Hamburg, Germany

Abstract

Optimising the slice energy spread in X-ray free electron lasers (XFELs) is key to their effective operation, and must be considered from the photoinjector at the very beginning of the machine. The standard approach, in which the measured beam size is entirely attributed to the product of the dispersion and the energy spread, has only a resolution on the order of several keV, meaning that a precise measurement in photoinjectors where the energy spread is predicted to be on the order of a few keV is challenging. However, recent techniques developed at SwissFEL, the Photo Injector Test Facility (PITZ) and at the European XFEL (EuXFEL) enable the slice energy spread to be determined with sub-keV precision. In this paper recent slice energy spread measurements at the EuXFEL are presented and contrasted with previous results. Furthermore its dependence on beamline parameters is explored. Finally, recent developments in the automation and simplification of the measurement procedure at the EuXFEL allow for a broader investigation of the slice energy spread and its dependence on the beamline configuration are stated.

INTRODUCTION

High-brightness electron beams are of fundamental importance at X-ray free electron laser facilities such as European X-ray Free Electron Laser (EuXFEL) [1, 2]. Efficient lasing in undulators at higher photon energies requires smaller slice energy spreads. Contrary to this requirement is the effect of the microbunching instability (MBI) upstream whereby a too-small slice energy spread upstream of the undulators can ultimately destroy the lasing [3, 4]. For this reason understanding the evolution of the slice energy spread of high-brightness electron beams in free electron lasers is of vital importance in order to ultimately further optimise their operation.

In recent years the slice energy spread in photoinjectors has been measured at several facilities, namely the SwissFEL [5, 6], the EuXFEL [7] and the Photo Injector Test Facility (PITZ) [8]. The slice energy spread is typically measured using a radio frequency transverse deflecting structure (TDS), thus streaking the beam and mapping the longitudinal phase space onto the transverse and then directly seen on a downstream screen in a dispersive section. The measured values for the slice energy spread in the aforementioned facilities were sufficiently small that numerous related novel methods were developed in order to sufficiently resolve them [5, 7, 8]. Of particular interest is the fact that three different facilities reported considerably different slice energy spreads in their respective photoinjectors, shown in Table 1, and all three are larger than anticipated by the theory. Furthermore Ref. [6] shows a relationship between the beamline optics (R_{56} and average β-functions) and the measured energy spread, explained in terms of MBI and intrabeam scattering (IBS), respectively. The R_{56} is generally constant in the injector but the β-functions are known to not be constant and vary over time. For example, typically after shutdowns the solenoid must be adjusted, resulting in different downstream β-functions, so that a variation in the energy spread after shutdowns might also be expected.

Table 1: Recent slice energy spread measurements in photoinjectors with key parameters alongside the measured σ_E. The latter SwissFEL result differs from the previous one due to differences in the lattice optics.

	SwissFEL 2020	SwissFEL 2022	EuXFEL 2021	PITZ 2022	Unit
σ_E	15	4	5.9	1.65	keV
Q	200		250	250	pC
E	100–400		130	20	MeV

In this paper recent developments involving the measurement and study of the slice energy spread in the injector at the EuXFEL are presented. In particular, a new set of measurements showing a considerably smaller value of the energy spread in the injector are reported. Furthermore a new tool for rapid data acquisition was used, and its application for a direct calibration for the energy spread induced by an upstream laser heater (LH) is shown.

METHOD

The injector needs to be specially configured for slice energy spread measurements. The TDS must be used to streak the beam upstream of the injector dump line where a screen is positioned at a point of non-zero dispersion D. The injector and dump line with the TDS and screen are shown in Fig. 1. At the downstream BC2 TDS where the energy spread is higher, relating the measured central slice width σ_M to the energy spread σ_E using $\sigma_E \approx E\sigma_M/D$ gives a sufficiently accurate result. However, this implicitly neglects the imaging resolution σ_R, the betatron component σ_B and the energy spread induced by the TDS $\sigma_{E,\mathrm{TDS}}$—all of which will increase the slice width σ_M. At sufficiently small slice energy spreads, such as in the injector, these contributions cannot be neglected. Accounting for these effects, a more accurate expression for the screen slice width can be given

* stuart.walker@desy.de

ISBN: 978-3-95450-231-8 ISSN: 2673-5490 doi: 10.18429/JACoW-IPAC2023-TUPL025

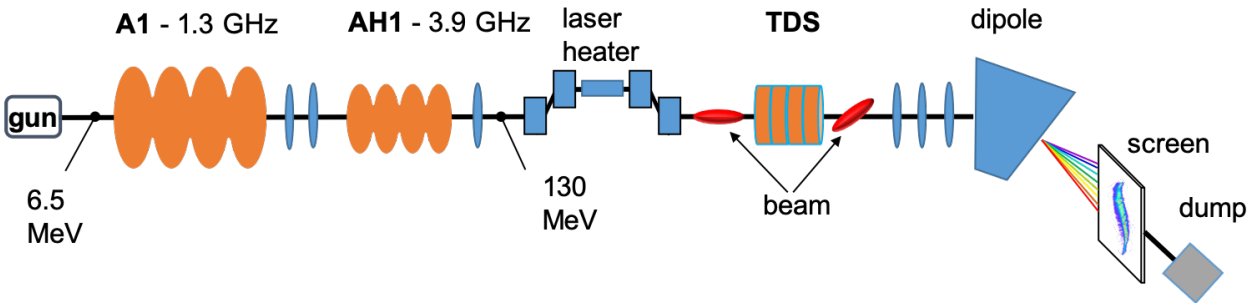

Figure 1: The EuXFEL injector and injector dumpline with key components highlighted. In the slice energy spread measurements AH1 and the laser heater are both typically switched off [7].

by

$$\sigma_M^2 = \sigma_R^2 + \sigma_B^2 + \frac{D^2}{E^2}(\sigma_E^2 + \sigma_{E,\mathrm{TDS}}^2). \quad (1)$$

The betatron component to the measured slice width and TDS contribution to the slice energy spread are given, respectively, by

$$\sigma_B^2 = \frac{\beta\varepsilon_n}{\gamma_0} \quad \text{and} \quad \sigma_{E,\mathrm{TDS}}^2 = eVk\sigma_I^2\,, \quad (2)$$

where the symbols have their usual meanings, k is the TDS wavenumber and σ_I is the beam size in the streaking plane in the TDS. Furthermore, a special set of optics are used so that the β at the screen can be fixed whilst varying D and also ensuring sufficient phase advance for streaking with the TDS. By keeping β fixed whilst varying either V or D, it is possible to express σ_M in terms of two equations

$$\sigma_M^2 = A_D + B_D D^2 \quad \text{and} \quad \sigma_M^2 = A_V + B_V V^2 \quad (3)$$

for fixed V and fixed D, respectively. In this way, by measuring the slice width σ_M whilst separately varying the TDS voltage V and the dispersion D at the screen, all the contributions to σ_M can be determined and the true energy spread σ_E can be calculated.

To further increase the resolution of the measurement, the high harmonic cavity, AH1, is switched off so that the effect of linear chirp does not contribute to the energy spread, whilst keeping the beam energy at the nominal injector energy of 130 MeV by adjusting the A1 voltage. The A1 phase is adjusted so that the highest energy slice is in the centre of the beam. This results in a characteristic crescent-shaped image on the screen. Disabling AH1 and adjusting A1's phase in this way has the added benefit of giving a well-defined and consistent choice of slice to measure: the highest energy slice, which generally will correspond to the centre of the beam. An example analysis for a single image is shown in Fig. 2, where the characteristic beam shape with the central slice highlighted can be seen alongside the Gaussian fit for the central width to obtain a value for σ_M. Lastly it must also be stated that to ensure the β at screen is correct, the central slice is matched using standard EuXFEL tooling [9].

Typically these measurements take a long time, on the order of one hour per measurement on top of about two hours to setup the machine. For this reason and so that the relationship between the slice energy spread and various machine and beam parameters can be studied, a new data analysis and measurement tool has been developed. The analysis implementation is independent of the one used in [7], and was validated on the same data. The image processing algorithms employed by the two implementations differ slightly and result in a difference in the results on the order of about 2 %.

RESULTS

The slice energy spread in the EuXFEL injector was first measured in February 2021 [7] and the measurement has subsequently been repeated several times since then, and it is these subsequent measurements that are described here. The November 2022 measurement—the first one taken since February 2021—was an attempt to recreate the machine conditions from that time as much as possible and also featured a β-scan at the screen to additionally resolve the slice emittance. The more recent energy spread measurement and the original one alongside other key derived parameters are shown in Table 2. It is immediately notable that the energy spread is considerably smaller now at 4.3 keV, and that all the other key parameters that contribute to the slice width at the screen remain the same as before. Only the slice energy spread, σ_E has changed, suggesting that new measurement was correct and the energy spread decrease is real. This measurement has been repeated several times since then and all measured values remain on the order of 4 keV as of April 2023.

The exact reason for this decrease is not immediately clear. Most notably the solenoid current has decreased (from 338 A to 326.6 A) as well as the gun gradient (from 56.7 MV m^{-1} to 54.7 MV m^{-1}) and gun phase (from −42.9° to −43.1°) changed in this time period, which will inevitably alter the betatron functions along the injector. The impact of the average betatron function on the slice energy spread due to IBS has already been demonstrated in Ref. [6]. Although these changes are relatively small (on the few % level), the impact of the emittance and beam sizes on IBS has been reported to be quite sensitive [10].

ISBN: 978-3-95450-231-8 ISSN: 2673-5490 doi: 10.18429/JACoW-IPAC2023-TUPL025

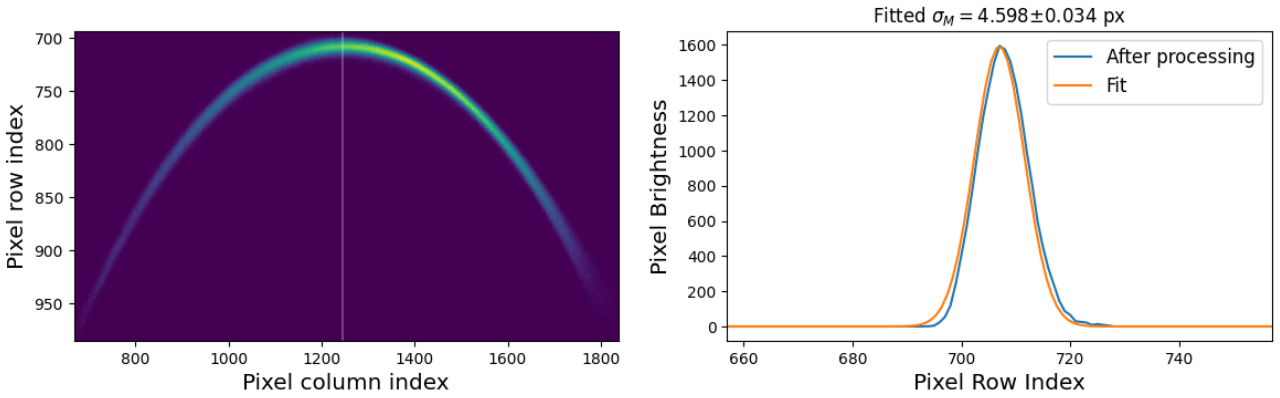

Figure 2: A typical screen image seen (left) in the injector energy spread measurements with image processing for the central slice (right). The background is subtracted from the raw image and the largest connected image "blob" is selected as the beam image. The beam is crescent-shaped because the third harmonic cavity, AH1, is disabled and the beam is on-crest in A1 (see Fig 1). This results in a large cubic chirp in the beam. The central slice is chosen for the measurement due to the absence of the cubic chirp in this portion.

Table 2: Two sets of slice energy spread measurements, the original result from [7] and a recent attempt at recreating the same machine conditions and measurement. The figure quoted here for the February 2021 result differs from the published result by about 2 % because a new analysis program has been written for this paper with a different image analysis pipeline.

Variable	Feb. 2021	Nov. 2022	Unit
σ_E	5.8(1)	4.3(1)	keV
σ_I	68.0(1)	64.0(8)	µm
σ_B	29.0(6)	28.0(4)	µm
σ_R	28.0(8)	27.0(5)	µm
ε_n	0.38(2)	0.34(9)	mm · mrad

LASER HEATER CALIBRATION

The laser heater (LH) in the injector is used to improve lasing in the downstream undulators by suppressing the MBI [11]. The laser interacts with the electron beam in a chicane to "heat" the beam—or more specifically to increase the slice energy spread. In daily operation the attenuation of the LH laser is simply adjusted until the pulse energy in the downstream undulators is at its maximum. However, the actual energy spread induced by the LH has never before been directly measured. Using the new fast data taking program outlined above, directly calibrating the LH is now possible. The measurement largely proceeded in the same way as before for a range of $\lambda/2$ plate rotation setpoints. However, at larger induced energy spreads it was impossible to ascertain the $\sigma_{E,\mathrm{TDS}}$ contribution, likely as it was relatively small in comparison with the LH contribution.

To resolve this, $\sigma_{E,\mathrm{TDS}}$ was calculated with the LH shutter closed and then used for all subsequent setpoints of the scan. By reexpressing Eq. (1) as a fixed term and a dispersion-dependent term as in Eq. (3), B_D can be measured at each setpoint and requires scanning only the dispersion. The explicit contribution of the LH is then given by Eq. (4), where σ_E^2 and $\sigma_{E,\mathrm{TDS}}^2$ are calculated with the LH shutter closed and B_D is measured at each dispersion setpoint.

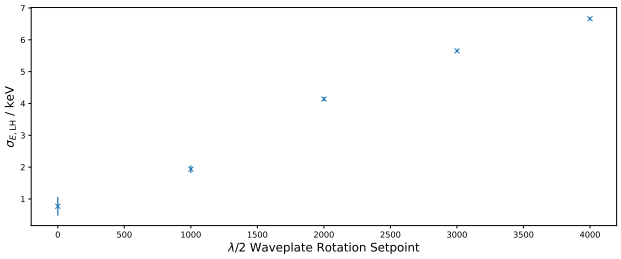

Figure 3: Induced energy spread for a range of half-wave plate rotation setpoints. The error bars are multiplied by three here to aid their visibility.

$$\sigma_{E,\mathrm{LH}} = \sqrt{E^2 B_D - \sigma_E^2 - \sigma_{E,\mathrm{TDS}}^2} \tag{4}$$

CONCLUSION

New energy spread measurements in the EuXFEL injector have been presented and discussed. Most notably, the energy spread is much smaller now at 4.3 keV in November 2022 than in the previous published result 5.8 keV from February 2021. To examine this possibility, it will be necessary to measure the energy spread regularly and routinely, meaning that the measurement must be as simple as possible. To this end a new code for measurement and online analysis is under active development and has been described. This will have the added benefit of enabling new explorations of beam and lattice properties on the energy spread, e.g. scanning the LH chicane R_{56} to explore MBI effects. One such application was demonstrated by providing an absolute calibration for the LH for the first time, however the LH alignment was not checked before the measurement and so the measurement should be repeated with a fully aligned LH in the future.

ISBN: 978-3-95450-231-8 ISSN: 2673-5490 doi: 10.18429/JACoW-IPAC2023-TUPL025

REFERENCES

[1] W. Decking *et al.*, "A MHz-repetition-rate hard X-ray free-electron laser driven by a superconducting linear accelerator", *Nat. Photonics*, vol. 14, no. 6, pp. 391–397, May 2020. doi:10.1038/s41566-020-0680-3

[2] R. Abela *et al.*, "XFEL: The European X-Ray Free-Electron Laser. Technical design report", Eds. M. Altarelli *et al.*, DESY, Hamburg, Germany, Tech. Rep. DESY-06-097, Jul. 2007. doi:10.3204/DESY_06-097

[3] Z. Huang and K.-J. Kim, "Formulas for coherent synchrotron radiation microbunching in a bunch compressor chicane", *Phys. Rev. ST Accel. Beams*, vol 5, no. 7, p. 074401, Jul. 2002. doi:10.1103/PhysRevSTAB.5.074401

[4] E. Saldin, E. Schneidmiller and M. Yurkov, "Klystron instability of a relativistic electron beam in a bunch compressor", *Nucl. Instrum. Methods Phys. Res., Sect. A* vol. 490, no. 1, pp. 1–8, Sep. 2002. doi:10.1016/S0168-9002(02)00905-1

[5] E. Prat, P. Dijkstal, E. Ferrari, A. Malyzhenkov, and S. Reiche "High-resolution dispersion-based measurement of the electron beam energy spread", *Phys. Rev. Accel. Beams*, vol. 23, no. 9, p. 090701, Sep. 2020. doi:10.1103/PhysRevAccelBeams.23.090701

[6] Eduard Prat *et al.*, "Energy spread blowup by intrabeam scattering and microbunching at the SwissFEL injector", *Phys. Rev. Accel. Beams*, vol. 25, no. 10, p. 104401, Oct. 2020. doi:10.1103/PhysRevAccelBeams.25.104401

[7] S. Tomin, I. Zagorodnov, W. Decking, N. Golubeva, and M. Scholz, "Accurate measurement of uncorrelated energy spread in electron beam", *Phys. Rev. Accel. Beams*, vol. 24, no. 6, p. 064201, Jun. 2020. doi:10.1103/PhysRevAccelBeams.24.064201

[8] Houjun Qian, *et al.*, "Slice energy spread measurement in the low energy photoinjector", *Phys. Rev. Accel. Beams*, vol. 25, no. 8, p. 083401, Aug. 2022. doi:10.1103/PhysRevAccelBeams.25.083401

[9] M. Scholz and B. Beutner, "Electron beam phase space tomography at the European XFEL injector", in *Proc. 8th Int. Particle Accelerator Conf. (IPAC'16)*, Copenhagen, Denmark, May 2016, pp. 196–198. doi:10.18429/JACoW-IPAC2017-MOPAB047

[10] P. Gjonaj, private communication, Apr. 2023.

[11] M. Hamberg and F. Brinker, "First heating with the European XFEL laser heater", in *Proc. 5th Int. Beam Instrum. Conf. (IBIC'16)*, Barcelona, Spain, Sep. 2016, pp. 694–696. doi:10.18429/JACoW-IBIC2016-WEPG32